

## Fractal-like Mechanical Resonators with a Soft-Clamped Fundamental Mode

S. A. Fedorov<sup>1</sup>,\* A. Beccari<sup>1</sup>, N. J. Engelsen<sup>1</sup>, and T. J. Kippenberg<sup>1</sup>†

*Institute of Physics (IPHYs), École Polytechnique Fédérale de Lausanne, 1015 Lausanne, Switzerland*

(Received 17 October 2019; published 16 January 2020)

Self-similar structures occur naturally and have been employed to engineer exotic physical properties. We show that acoustic modes of a fractal-like system of tensioned strings can display increased mechanical quality factors due to the enhancement of dissipation dilution. We describe a realistic resonator design in which the quality factor of the fundamental mode is enhanced by as much as 2 orders of magnitude compared to a simple string with the same size and tension. Our findings can open new avenues in force sensing, cavity quantum optomechanics, and experiments with suspended test masses.

DOI: 10.1103/PhysRevLett.124.025502

**Introduction.**—Self-similar structures can have unusual physical properties. Coastlines are a famous example—their length is loosely defined at geographic scale [1]. In the domain of optics, it was found that self-similar cavities can support modes with an arbitrarily small mode volume [2] at a given wavelength. Meanwhile, hierarchical metamaterials can have improved stiffness per unit mass [3,4] compared to natural materials. The acoustic vibrations of resonators are also known to be affected by structural self-similarity in a nontrivial way, in terms of both the vibrational mode density [5,6] and damping [7]. The latter can aid the design of mechanical resonators with low dissipation.

In this Letter, we study mechanical vibrations of systems of tensioned strings in the shape of self-similar binary trees, which are clamped at the tips in order to sustain tension [see Fig. 1(a)]. In such structures, owing to the combination of a high aspect ratio and static stress, the intrinsic loss-limited quality factors ( $Q$ 's) of flexural modes are controlled by dissipation dilution [8–10]. The diluted  $Q$  of a resonator mode is related to the material loss angle  $\phi$  (the phase delay between stress and strain) as [8–12]

$$Q = D_Q / \phi. \quad (1)$$

The dissipation dilution coefficient,  $D_Q$ , can be much greater than 1 and is quite generally found to be [8–12]

$$D_Q = \frac{\langle W_{\text{total}} \rangle}{\langle W_{\text{lossy}} \rangle} = \frac{1}{\alpha\lambda + \beta\lambda^2}. \quad (2)$$

Here  $\langle W_{\text{total}} \rangle$  is the dynamic elastic energy averaged over the vibrational period,  $\langle W_{\text{lossy}} \rangle$  is its lossy part, and the parameter  $\lambda = h/l\sqrt{E/(12\sigma)}$  depends on the resonator length,  $l$ , thickness in the direction of deformation,  $h$ , Young's modulus,  $E$ , and static stress,  $\sigma$ . The two terms in the denominator of Eq. (2), which scale differently with  $\lambda$ , come from the integration of lossy energy over the

resonator's clamped boundary and the bulk. We call  $\alpha$  and  $\beta$  the boundary and distributed loss coefficients, respectively.

Self-similar binary trees can be used to realize resonators with dramatically enhanced quality factors of the fundamental mode. When propagating over the hierarchy of branchings, flexural modes reduce in amplitude, which can suppress the boundary loss coefficient,  $\alpha$ , and make the modes “soft clamped” [13]. To date, the only known example of soft-clamped modes are modes localized around defects in stressed phononic crystals (PnC) [13,14]. This method, in combination with engineering of stress concentration, resulted in a demonstration of quality factors approaching  $10^9$  [14] in  $\text{Si}_3\text{N}_4$  nanomechanical resonators at room temperature. However, the PnC localization approach has an inherent limitation, which

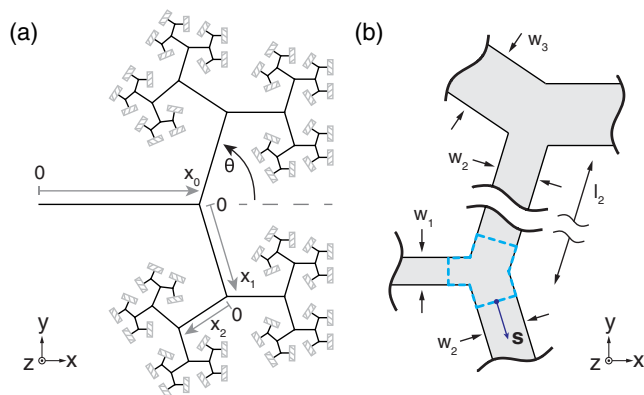


FIG. 1. (a) Binary tree with six branching levels. Local  $x$  coordinates are shown for the first three levels. One tree defines half a resonator, and the complete structure is formed by adding its mirror reflection in the  $yz$  plane. Hatched rectangles indicate clamping points. (b) Two branching points of a binary-tree resonator with the definitions of the segment widths,  $w$ , and lengths,  $l$ . The dashed blue contour is used to derive the transformation of the mode derivative.

makes it disadvantageous in many potential applications— it applies only to high-order modes of the suspended structure. In contrast, our self-similar structures can realize low-order modes with unprecedented quality factors, complementing other known methods of engineering dissipation dilution [12–16].

Our results are relevant to areas ranging from sensing [17,18] to cavity quantum optomechanics [19], which employ stressed, high- $Q$  nanomechanical resonators [20–22]. Moreover, because of the close relationship between the  $Q$  of the fundamental mode of a clamped tensioned structure and the  $Q$  of a pendulum [8], our results can be used for designing high- $Q$  suspensions of test masses, akin to those employed in gravitational wave detectors and experiments on macroscopic optomechanics [23–25].

This Letter is structured as follows. First we show how the propagation of a flexural mode across a string branch point reduces the boundary loss coefficient and present a theory of binary-tree resonators that incorporate cascaded branchings. We calculate the  $Q$ 's of a sample  $\text{Si}_3\text{N}_4$  nanoresonator and predict a fundamental mode  $Q$  exceeding  $10^9$  assuming experimentally realistic parameters. We then study the variation of boundary and distributed loss coefficients with the parameters of the binary trees and show that the trade-off for a reduction of boundary loss is an increase in the distributed loss.

*Boundary losses.*—We start by reviewing the relation between the boundary loss coefficient,  $\alpha$ , and the mode amplitude gradient. The transverse displacement field  $u(x)$  of a flexural string mode in the high-tension limit is found from the equation

$$-\sigma(x) \frac{d^2 u}{dx^2} = \omega^2 \rho u, \quad (3)$$

where  $x$  is the coordinate along the string,  $\sigma(x) \equiv \sigma_{xx}(x)$  is the static axial stress distribution,  $\rho$  is the material density, and  $\omega$  is the mode frequency. Equation (3) is valid everywhere except in the regions close to the string clamping points. Once the standing wave approaches a clamping point, it enters a transition region over which it reduces its gradient to zero. In the vicinity of the clamped boundary, the mode experiences sharp bending with curvature given by (see the Supplemental Material of Ref. [12], and also Refs. [8,11])

$$u''_{\text{cl}}(x) = \frac{u'(+0)}{\lambda_{\text{cl}} l} \exp\left(-\frac{x}{\lambda_{\text{cl}} l}\right), \quad (4)$$

where the clamping point is at  $x = 0$  [such that  $u(0) = 0$ ], the string extends to  $x > 0$ , and  $u'(+0)$  is the derivative of the solution of Eq. (3) which does not satisfy the boundary condition  $u'(0) = 0$ . The parameter  $\lambda_{\text{cl}}$  is defined with  $h$  and  $\sigma$  local to the clamp [15]. The total lossy elastic energy is commonly dominated by the contribution from the

clamps [9,11], and since this contribution is proportional to the integral of the mode curvature squared, it is decreased by the reduction of  $u'(+0)$ .

*Propagation across a branch point.*—An interesting situation in which suppression of the flexural mode gradient occurs is when a string mode propagates over a branch point. In order to show this, we consider a junction of three beams with rectangular cross section, highlighted by the blue contour in Fig. 1(b). The dynamic equation for the two-dimensional profile of out-of-plane vibrations  $u(x, y)$  is given by [26]

$$-\frac{\partial}{\partial x_i} \left( \sigma_{ij} \frac{\partial u}{\partial x_j} \right) = \omega^2 \rho u, \quad (5)$$

which generalizes Eq. (3). We assume summation over the repeating indices  $i$  and  $j$ , each of which runs over the two spatial coordinates,  $x$  and  $y$ . The components of the stress tensor  $\sigma_{ij}$  are functions of  $x$  and  $y$ . By integrating both sides of Eq. (5) over the infinitesimally small area of the contour and transforming the divergence into a boundary integral, we find that

$$\oint ds_i \left( \sigma_{ij} \frac{\partial u}{\partial x_j} \right) = 2w_2 \sigma_2 u'_2 - w_1 \sigma_1 u'_1 = 0, \quad (6)$$

where  $u'_1$  and  $u'_2$  are the amplitude gradients in the directions of axes  $x_1$  and  $x_2$ , respectively. We assumed that the mode branches symmetrically and correspondingly doubled the contribution of  $u'_2$ . Next, the balance of static tensile forces requires

$$w_1 \sigma_1 = 2w_2 \sigma_2 \cos(\theta). \quad (7)$$

Combining Eqs. (6) and (7), we find that

$$u'_2 = u'_1 \cos(\theta). \quad (8)$$

Equation (8) shows that the mode gradient is reduced by a factor of  $\cos(\theta)$  after propagating over a branch point. Although the reduction in principle can be arbitrarily large if  $\theta$  is close to  $\pi/2$ , the improvement in dissipation dilution provided by a single branch point is fairly limited. The reason for this is an associated increase in the distributed lossy energy caused by the torsional deformation of the beams. Nevertheless, we will show that cascaded branchings can greatly reduce residual lossy energy.

*Self-similar binary-tree resonators.*—Multiple string branchings can be cascaded such that their totality forms a binary tree, as shown in Fig. 1. After each branching, the lengths of the string segments are reduced by the same ratio in order to prevent self-overlap. As realistic resonators have to be hard clamped on all sides, we consider structures composed of two symmetric binary trees joined at the roots and clamped at the tips. We treat the case in which all of the

strings are beams with rectangular cross section and the same thickness, as this geometry is potentially suitable for nanofabrication. Our main qualitative results, however, are not contingent on this assumption. Since we are primarily interested in the fundamental resonator mode, in the following, we theoretically consider only the modes that split symmetrically at each branch point.

Binary-tree resonators are convenient to analyze using a set of local axes,  $x_n$ , each directed along one segment, beginning at one branch point and ending at the next one as shown in Fig. 1(a). Considering one path from the resonator center to one of the clamps is sufficient for describing symmetrically split modes. We index the branching level by  $n$ , starting from  $n = 0$  for the central segment. The total number of branchings is denoted by  $N$ . The flexural deformation of each segment as a function of the local coordinate is denoted by  $u_n(x_n)$ . The segment lengths,  $l_n$ , and widths,  $w_n$  [shown in Fig. 1(b)], are found using the ratios  $r_l$  and  $r_w$  as  $l_n = l_0(r_l)^n$  and  $w_n = w_0(r_w)^n$ , respectively.

Flexural modes of tree resonators can be found by matching the solutions  $u_n(x_n)$  over different segments using Eq. (8), the continuity condition  $u_n(l_n) = u_{n+1}(0)$ , and the boundary conditions  $u_N(l_N) = 0$  and  $u'_0(0) = 0$  [or  $u_0(0) = 0$ ]. With  $u_n(x_n)$  in hand, one can compute the dissipation dilution factors, and the loss coefficients  $\alpha$  and  $\beta$ . However, we need to introduce one more concept before we can provide explicit expressions for these quantities.

*Torsional lossy energy.*—Flexural deformations of a two-dimensional system of strings in general induce torsional deformation of the segments. If the segments have high aspect ratios, torsion does not produce geometrically nonlinear strain in the direction of the string axis [12] and contributes only to the lossy elastic energy.

The emergence of torsion in a tree segment is illustrated in the inset of Fig. 2(a). The equilibria of force moments at the junctions define the boundary conditions for the torsion angles. At the beginning of the segment, the angle is set by the previous segment as  $\tau_n = u'_{n-1}(l_{n-1}) \sin(\theta)$ . At the end of the segment, the angle is zero. The torsional energy stored by one segment is then given by

$$\langle W_{\text{tors}} \rangle_n = \frac{E w_n h^3}{6(1 + \nu)} \int_0^{l_n} dx_n [\tau'(x_n)]^2, \quad (9)$$

where  $\nu$  is Poisson's ratio. If the aspect ratio of the segment is high (which we assume in the following), the transition from  $\tau_n$  to zero happens linearly, and  $\tau' = \tau_n/l_n$ .

Note that if the full resonator can be modeled as a patterned 2D membrane, one can use the general formula of the Supplemental Material of Ref. [11] to find the lossy energy, including the contribution which we refer to as ‘‘torsional.’’ Nevertheless, we find it useful to separate the torsional energy, as this concept is generalizable to strings

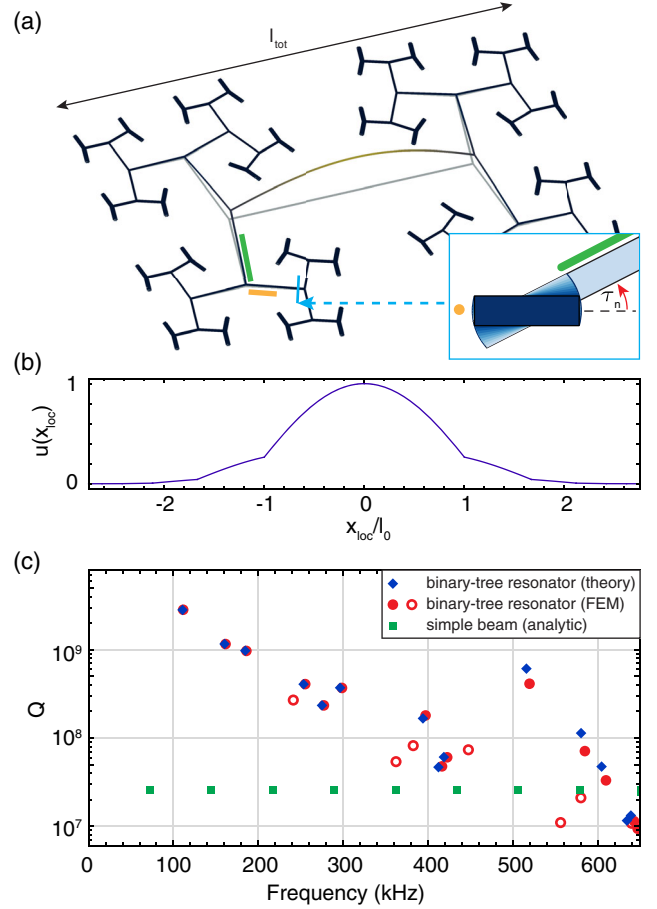


FIG. 2. (a) FEM simulation of the fundamental mode of a stress-preserving binary-tree resonator. (Inset) Schematic display of a cut view of one segment (marked with orange) and illustration of the torsion created by the previous segment (marked with green). (b) The displacement of the mode shown in (a) plotted over the local  $x$  coordinates. (c) Quality factors and frequencies of out-of-plane modes of the resonator shown in (a). Blue diamonds correspond to the theory presented in this Letter, red dots to the result of FEM simulation. Filled red circles, symmetrically branched modes; empty circles, other modes. Green squares show out-of-plane modes of a doubly clamped beam resonator with the same  $l_{\text{tot}}$ .

with nonrectangular cross sections for which the relation to membranes is not obvious.

*Quality factors and loss coefficients.*—The quality factors of intrinsic loss-limited resonator modes are found by using Eqs. (1) and (2). The energies involved are calculated by summing up the contributions from all of the tree segments. The lossless ‘‘tension’’ energy is given by

$$\langle W_{\text{tens}} \rangle = 2 \sum_{n=0}^N 2^n \sigma_n w_n h \int_0^{l_n} dx_n [u'_n(x_n)]^2. \quad (10)$$

The lossy energy consists of three contributions

$$\langle W_{\text{lossy}} \rangle = \langle W_{\text{bend,b}} \rangle + \langle W_{\text{bend}} \rangle + \langle W_{\text{tors}} \rangle. \quad (11)$$

The distributed bending energy is

$$\langle W_{\text{bend}} \rangle = 2 \sum_{n=0}^N 2^n \frac{E W_n h^3}{12} \int_0^{l_n} dx_n [u_n''(x_n)]^2, \quad (12)$$

while the boundary bending is

$$\langle W_{\text{bend,b}} \rangle = 2^N W_N h^2 \sqrt{\frac{E}{12}} \sqrt{\sigma_N [u_N'(l_N - 0)]^2}, \quad (13)$$

and the torsional contribution is

$$\langle W_{\text{tors}} \rangle = 2 \sum_{n=1}^N 2^n \frac{E W_n h^3}{6(1+\nu)l_n} [u_{n-1}'(l_{n-1}) \sin(\theta)]^2. \quad (14)$$

The loss coefficients in Eq. (2) are identified as

$$\alpha = \frac{\langle W_{\text{bend,b}} \rangle}{\lambda \langle W_{\text{tens}} \rangle}, \quad (15)$$

$$\beta = \frac{\langle W_{\text{bend}} \rangle + \langle W_{\text{tors}} \rangle}{\lambda^2 \langle W_{\text{tens}} \rangle} = \beta_{\text{bend}} + \beta_{\text{tors}}. \quad (16)$$

Note that  $\alpha$  and  $\beta$  are independent of  $\lambda$ , which in our case is defined as

$$\lambda = \frac{h}{l_{\text{tot}}} \sqrt{\frac{E}{12\sigma_0}}, \quad (17)$$

with  $l_{\text{tot}}$  being the total resonator size in the direction along the central segment. Given  $l_0$ ,  $r_l$ , and  $\theta$ , one can find  $l_{\text{tot}}$  analytically, but the resulting expression is cumbersome.

*Stress-preserving trees.*—The distribution of static stress in a binary-tree resonator in general can be such that the stress is peaked either in the branch tips or in the trunk. For simplicity, we restrict our numeric analysis to the trees in which the static stress along the segments is uniform. As follows from the balance of static forces [Eq. (7)], the condition  $\sigma_{n+1} = \sigma_n$  is fulfilled (and the resonator is “stress preserving”) if the width scaling ratio is set to  $r_w = 1/[2 \cos(\theta)]$ . If a stress-preserving resonator is patterned from a film with isotropic initial prestress, denoted as  $\sigma_{\text{film}}$ , upon suspension, the static stress in all segments is given by

$$\sigma_n = \sigma_{\text{film}}(1 - \nu). \quad (18)$$

*Simulation results.*—The basic acoustic properties of binary-tree resonators can be understood by giving an example. In Fig. 2, we present a simulation of a stress-preserving resonator with five branching levels,  $r_l = 0.67$ ,  $l_0 = 1$  mm ( $l_{\text{tot}} = 3.7$  mm),  $w_0 = 100$  nm,  $h = 20$  nm,

$\theta = 80$  deg, which is made of high-stress stoichiometric silicon nitride film ( $\sigma_{\text{film}} = 1.14$  GPa,  $E = 250$  GPa,  $\nu = 0.23$ ,  $\rho = 3100$  kg/m<sup>3</sup>,  $1/\phi = 1.4 \times 10^3$  [14]) at room temperature. The assumed loss angle of the film is much larger than the loss achievable in bulk material due to surface losses [27].

The fundamental resonator mode is shown in Figs. 2(a) and 2(b). The reduction of mode amplitude gradient at each branch point can be observed from these figures. Note that the apparent discontinuity of the mode derivative in Fig. 2(b) is due to the turns of the path following the local  $x$  axes—the two-dimensional mode has no sharp bends at the branch points.

The calculated quality factors are presented in Fig. 2(c), which shows that the  $Q$  of the fundamental mode is enhanced by about 2 orders in magnitude compared to a simple doubly clamped beam of the same size. All low-frequency flexural modes experience similar  $Q$  enhancement, which gradually decreases with an increase in frequency.

Two methods were used to obtain the data in Fig. 2(c): the theory presented in this Letter, which relies on the one-dimensional approximation of segment modes, and a finite-element method (FEM) simulation of a nonuniform plate under tension. The frequencies and quality factors found using different methods agree within a few percent for a few lower-order modes, whereas higher-order modes show higher discrepancy due to the onset of hybridization between bending and torsion (neglected in our theoretical analysis). The FEM simulation also provides information about the in-plane and nonsymmetrically branched modes of the structure. For clarity, we do not show in-plane modes in Fig. 2(c), as their quality factors are significantly lower than the out-of-plane modes, while their density is about the same.

In order to obtain a more general insight, we study the variation of loss coefficients  $\alpha$  and  $\beta$  (which are material and size independent) of the fundamental resonator mode with the geometric parameters  $r_l$ ,  $r_w$ ,  $\theta$ , and  $N$ . We keep  $r_w$  fixed to satisfy the stress-preservation condition at given  $\theta$ . Furthermore, we put  $r_l = r_{l,\text{crit}}(\theta)$ , where  $r_{l,\text{crit}}$  is the value at which tip-to-tip self-contact occurs in a fractal tree with infinite  $N$  (and there is no self-contact for finite  $N$ ). We sweep the remaining free parameters,  $\theta$  and  $N$ , and present the results in Fig. 3. It can be seen that  $\alpha$  is suppressed as  $\theta$  increases, while  $\beta_{\text{tors}}$ , on the contrary, goes up. Therefore, the torsional lossy energy eventually becomes the main limitation for dissipation dilution as the boundary loss is suppressed. The exact parameters at which the overall dissipation dilution factor is maximized depend on  $\lambda$ —for smaller  $\lambda$ , the optimum shifts toward larger  $\theta$  or  $N$ .

*Fractal limit.*—The data in Fig. 3 help us to understand some properties of binary-tree resonators in the fractal limit when  $N$  goes to infinity. As  $N$  increases,  $\alpha$  reduces to zero, and  $\beta_{\text{bend}}$  converges to a finite value. The distributed torsion

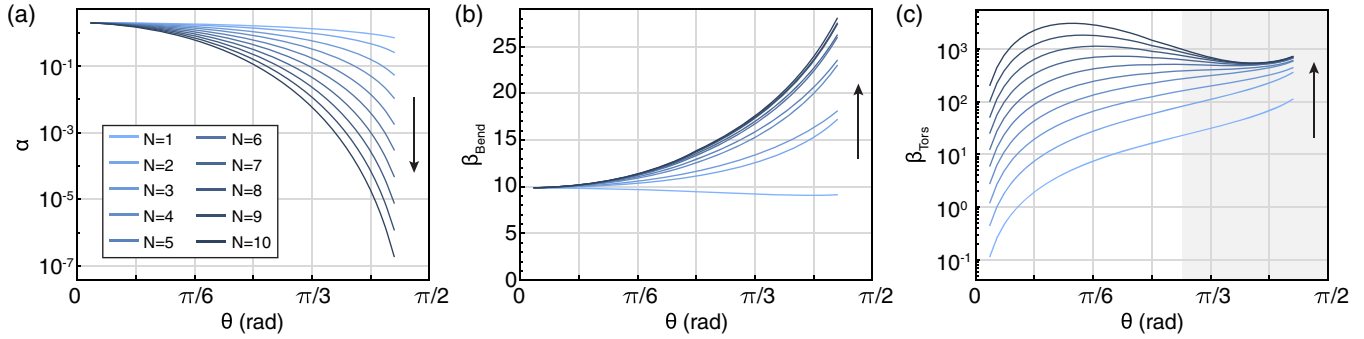


FIG. 3. Loss coefficients for stress-preserving binary-tree resonators with  $r_l = r_{l,\text{crit}}(\theta)$  and different numbers of branchings  $N$ . (a) Boundary loss coefficient. (b) Distributed bending loss coefficient. (c) Distributed torsional loss coefficient. The region where  $\beta_{\text{tors}}$  converges with increasing  $N$  is shaded gray. The direction of increasing  $N$  is also indicated by arrows in the plots.

loss coefficient  $\beta_{\text{tors}}$  has more complex behavior with increasing  $N$ , it can either converge to a finite value or increase indefinitely. Which of the two scenarios is realized depends on the behavior of geometric series in Eq. (14), which can be shown to converge if  $\cos(\theta) < \sqrt{r_l/(2r_w)}$ . Correspondingly, the  $Q$  of the fundamental mode of a fractal structure either can be finite and limited by the distributed energy loss or it can be low and can approach the undiluted value  $1/\phi$ .

*Potential experimental realization.*—High-stress mechanical resonators with complex shapes, millimeter-scale length, and thickness down to 20 nm were successfully fabricated recently [13,14,28] from silicon nitride films deposited by low pressure chemical vapor deposition on silicon. It is likely that our proposed geometries with the dimensions assumed in Fig. 2 can be fabricated using the same processes. Our resonators must be operated at pressure below  $10^{-8}$  mbar in order to prevent gas damping of the vibrational modes [29]. The measurement of the resonator modes with thermal-noise limited displacement sensitivity should be possible using common optical interferometric techniques [13,14,28]. The resonators also can be probed by coupling them with whispering gallery mode resonators [30,31], photonic crystal cavities [32,33], and superconducting circuits [34,35].

*Conclusions and outlook.*—We showed that the boundary contribution to the lossy elastic energy of flexural modes can be suppressed in a system of tensioned strings connected to form a self-similar tree. This boundary loss suppression does not require the structure to extend beyond one acoustic wavelength and therefore can enhance the quality factor of the fundamental resonator mode, as well as of a multitude of other low-order modes at the same time. Our results are relevant to the design of beam and tethered-membrane [18,28] nanomechanical resonators, as well as the suspensions of macroscopic test masses [23–25].

The code to reproduce the data in Figs. 2 and 3 is available on Zenodo [36].

The authors thank Alexander Tagantsev and Vivishek Sudhir for their comments on the manuscript. This work was supported by the Swiss National Science Foundation under Grant No. 182103 and the Defense Advanced Research Projects Agency (DARPA), Defense Sciences Office (DSO), under Contract No. D19AP00016 (QUORT). A. B. acknowledges support from the European Union’s Horizon 2020 research and innovation program under Marie Skłodowska-Curie Grant Agreement No. 722923 (OMT). N. J. E. acknowledges support from the Swiss National Science Foundation under Grant No. 185870 (Ambizione).

\*sergey.fedorov@epfl.ch

†tobias.kippenberg@epfl.ch

- [1] B. Mandelbrot, *Science* **156**, 636 (1967).
- [2] H. Choi, M. Heuck, and D. Englund, *Phys. Rev. Lett.* **118**, 223605 (2017).
- [3] R. Lakes, *Nature (London)* **361**, 511 (1993).
- [4] D. Rayneau-Kirkhope, Y. Mao, and R. Farr, *Phys. Rev. Lett.* **109**, 204301 (2012).
- [5] S. Alexander and R. Orbach, *J. Phys. (Paris), Lett.* **43**, 625 (1982).
- [6] B. Sapoval, T. Gobron, and A. Margolina, *Phys. Rev. Lett.* **67**, 2974 (1991).
- [7] B. Sapoval, O. Haerberlé, and S. Russ, *J. Acoust. Soc. Am.* **102**, 2014 (1997).
- [8] G. I. González and P. R. Saulson, *J. Acoust. Soc. Am.* **96**, 207 (1994).
- [9] Q. P. Unterreithmeier, T. Faust, and J. P. Kotthaus, *Phys. Rev. Lett.* **105**, 027205 (2010).
- [10] S. Schmid, K. D. Jensen, K. H. Nielsen, and A. Boisen, *Phys. Rev. B* **84**, 165307 (2011).
- [11] P.-L. Yu, T. P. Purdy, and C. A. Regal, *Phys. Rev. Lett.* **108**, 083603 (2012).
- [12] S. A. Fedorov, N. J. Engelsen, A. H. Ghadimi, M. J. Beryhi, R. Schilling, D. J. Wilson, and T. J. Kippenberg, *Phys. Rev. B* **99**, 054107 (2019).
- [13] Y. Tsaturyan, A. Barg, E. S. Polzik, and A. Schliesser, *Nat. Nanotechnol.* **12**, 776 (2017).

- [14] A. H. Ghadimi, S. A. Fedorov, N. J. Engelsen, M. J. Beryhi, R. Schilling, D. J. Wilson, and T. J. Kippenberg, *Science* **360**, 764 (2018).
- [15] M. J. Beryhi, A. Beccari, S. A. Fedorov, A. H. Ghadimi, R. Schilling, D. J. Wilson, N. J. Engelsen, and T. J. Kippenberg, *Nano Lett.* **19**, 2329 (2019).
- [16] P. Sadeghi, M. Tanzer, S. L. Christensen, and S. Schmid, *J. Appl. Phys.* **126**, 165108 (2019).
- [17] D. Garcia-Sanchez, K. Y. Fong, H. Bhaskaran, S. Lamoreaux, and H. X. Tang, *Phys. Rev. Lett.* **109**, 027202 (2012).
- [18] R. Fischer, D. P. McNally, C. Reetz, G. G. T. Assumpo, T. Knief, Y. Lin, and C. A. Regal, *New J. Phys.* **21**, 043049 (2019).
- [19] M. Aspelmeyer, T. J. Kippenberg, and F. Marquardt, *Rev. Mod. Phys.* **86**, 1391 (2014).
- [20] S. S. Verbridge, J. M. Parpia, R. B. Reichenbach, L. M. Bellan, and H. G. Craighead, *J. Appl. Phys.* **99**, 124304 (2006).
- [21] B. M. Zwickl, W. E. Shanks, A. M. Jayich, C. Yang, A. C. Bleszynski Jayich, J. D. Thompson, and J. G. E. Harris, *Appl. Phys. Lett.* **92**, 103125 (2008).
- [22] Q. P. Unterreithmeier, E. M. Weig, and J. P. Kotthaus, *Nature (London)* **458**, 1001 (2009).
- [23] T. Corbitt, D. Ottaway, E. Innerhofer, J. Pelc, and N. Mavalvala, *Phys. Rev. A* **74**, 021802(R) (2006).
- [24] T. Corbitt, C. Wipf, T. Bodiya, D. Ottaway, D. Sigg, N. Smith, S. Whitcomb, and N. Mavalvala, *Phys. Rev. Lett.* **99**, 160801 (2007).
- [25] T. Bodiya, V. Sudhir, C. Wipf, N. Smith, A. Buikema, A. Kontos, H. Yu, and N. Mavalvala, *Phys. Rev. A* **100**, 013853 (2019).
- [26] L. D. Landau and E. M. Lifshitz, *Theory of Elasticity* (Pergamon Press, London, 1970).
- [27] L. G. Villanueva and S. Schmid, *Phys. Rev. Lett.* **113**, 227201 (2014).
- [28] C. Reinhardt, T. Müller, A. Bourassa, and J. C. Sankey, *Phys. Rev. X* **6**, 021001 (2016).
- [29] M. J. Martin, B. H. Houston, J. W. Baldwin, and M. K. Zalalutdinov, *J. Microelectromech. Syst.* **17**, 503 (2008).
- [30] G. Anetsberger, O. Arcizet, Q. P. Unterreithmeier, R. Rivire, A. Schliesser, E. M. Weig, J. P. Kotthaus, and T. J. Kippenberg, *Nat. Phys.* **5**, 909 (2009).
- [31] R. Schilling, H. Schütz, A. H. Ghadimi, V. Sudhir, D. J. Wilson, and T. J. Kippenberg, *Phys. Rev. Applied* **5**, 054019 (2016).
- [32] A. G. Krause, M. Winger, T. D. Blasius, Q. Lin, and O. Painter, *Nat. Photonics* **6**, 768 (2012).
- [33] J. Guo, R. Norte, and S. Gröblacher, *Phys. Rev. Lett.* **123**, 223602 (2019).
- [34] M. Yuan, M. A. Cohen, and G. A. Steele, *Appl. Phys. Lett.* **107**, 263501 (2015).
- [35] J. M. Fink, M. Kalae, A. Pitanti, R. Norte, L. Heinzle, M. Davano, K. Srinivasan, and O. Painter, *Nat. Commun.* **7**, 12396 (2016).
- [36] The Mathematica notebook is available at <http://dx.doi.org/10.5281/zenodo.3496611>.